Structured Surfaces for a Giant Liquid Slip

Choongyeop Lee,[1] Chang-Hwan Choi,[2] and Chang-Jin "CJ" Kim[1]

[1]*Mechanical and Aerospace Engineering Department, University of California, Los Angeles (UCLA), California 90095, USA*
[2]*Department of Mechanical Engineering, Stevens Institute of Technology, New Jersey 07030, USA*

We study experimentally how two key geometric parameters (pitch and gas fraction) of textured hydrophobic surfaces affect liquid slip. The two are independently controlled on precisely fabricated microstructures of posts and grates, and the slip length of water on each sample is measured using a rheometer system. The slip length increases linearly with the pitch but dramatically with the gas fraction above 90%, the latter trend being more pronounced on posts than on grates. Once the surfaces are designed for very large slips (>20 μm), however, further increase is not obtained in regular practice because the meniscus loses its stability. By developing near-perfect samples that delay the transition from a dewetted (Cassie) to a wetted (Wenzel) state until near the theoretical limit, we achieve giant slip lengths, as large as 185 μm.

Liquid slip on a solid surface has recently been explored extensively in part for its application possibilities in nano- and microsystems [1]. Slip length—a measure of slip defined as the ratio of slip velocity to shear rate at the wall—amounts to typically tens of nanometers over *smooth* surfaces, mostly hydrophobic [1], limiting such a slip's relevance only to nanoscale flow systems [2]. Meanwhile, a *textured* hydrophobic surface can create a composite (solid and gas) interface with the liquid, demonstrating a superhydrophobicity and, in an extreme case of a near 180° contact angle, a dramatic ($>99\%$) friction reduction for sliding *droplets* [3]. In addition, an enhanced liquid slippage on these superhydrophobic surfaces has been demonstrated experimentally [4–10] and numerically [11–19] in recent years, including a direct reporting of slip lengths over 20 μm [7,9]. In particular, for the experimental studies, several surfaces were examined, including random [4–6], semiregular [7,8], and regular patterns [9,10]. However, these studies did not clarify the key roles of individual geometric surface parameters on the slippage effect, which is critical to engineer the surfaces for desired applications such as frictional drag reduction. In this study, we investigate the independent effects of two key surface parameters—structural pitch (periodicity) and gas fraction—by developing well-defined and defect-free microstructured surfaces. The systematic investigation leads us to optimize the surface parameters for maximum slip effects.

In order for a superhydrophobic surface to produce a large effective slip in most real practices, the surface should maintain a dewetted (fakir) state even under a pressurized flow condition. The transition mechanism from a dewetted (Cassie) to a wetted (Wenzel) state can be explained by the minimization of thermodynamic free energy [20] or by the force balance between a surface tension and the pressure across the interface [21]. Based on the force balance approach [21], we calculated the maximum gas fraction that is maintainable at a given pitch

and applied pressure, as shown in Fig. 1, to design the surface structures for this study. Here the stability condition (i.e., sustaining a Cassie state) for posts is given by

$$P_l \phi_g \leq -4\gamma(1 - \phi_g)\cos\theta/D, \tag{1}$$

where P_l is the liquid pressure over a gas, ϕ_g is a gas fraction, γ is the surface tension of a liquid (72×10^{-3} N/m for water at 25 °C), θ is the contact angle of a liquid on a flat surface (~120° for a water droplet on Teflon), and D is the top diameter of a post. For grates,
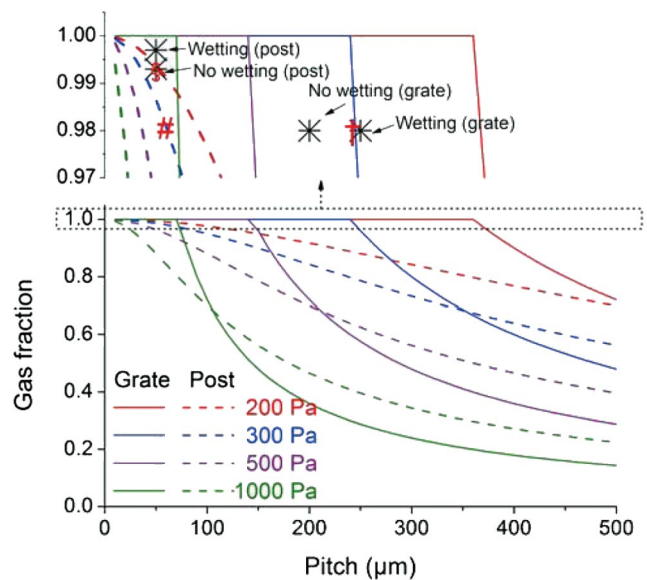
FIG. 1 (color). Maximum gas fraction for a dewetted (Cassie) surface condition for posts (dashed lines) and grates (solid lines). Liquid pressure and structural pitch determine the maximum gas fraction allowable without the transition from nonwetting to wetting. The stability condition is also dependent on the configuration of underlying patterns (e.g., posts vs grates). The inset magnifies the high gas fraction region, showing key data points theoretical and experimental.

the stability condition is given by

$$P_l \phi_g \leq -2\gamma \cos\theta / L, \tag{2}$$

where L is the pitch. As expected, Fig. 1 indicates that the maximal sustainable gas fraction for a Cassie state decreases as the liquid pressure increases or the pitch of the surface pattern increases. More instructive is to note that, for a given pressure (e.g., 500 Pa), grate patterns allow a higher gas fraction for small pitches (e.g., <200 μm) while post patterns allow a higher gas fraction for large pitches (e.g., >200 μm).

A commercial rheometer (AR 2000, TA Instruments) with a cone-and-plate arrangement [Fig. 2(a)] was utilized to measure the torque over the samples and calculate the slip lengths [7,22]. A stainless-steel cone with 60 mm diameter, 2° cone angle, and 53 μm truncation was used. Deionized (DI) water was used as a test liquid maintained at 25 ± 0.1 °C by a Peltier plate during all of the tests. The torque M was recorded in the shear rate ranging 90–130 s^{-1} and was converted to the slip length δ using the mathematical relationship represented by

$$M = \frac{2\pi\mu\Omega R^3}{3\theta_0} \left[1 - \frac{3\delta}{2R\theta_0} + \frac{3\delta^2}{R^2\theta_0^2} - \frac{3\delta^3}{R^3\theta_0^3} \right.$$
$$\left. \times \ln\left(\frac{R\theta_0 + \delta}{\delta}\right) \right], \tag{3}$$

where μ is a liquid viscosity (8.94×10^{-4} Pa s for water at 25 °C) and R, Ω, and θ_0 are a cone radius, the angular velocity of the cone, and the cone angle, respectively [23].

For superhydrophobic surface samples, well-regulated post or grate structures on a micrometer scale were created over a 60 mm-diameter circular area on a 100 mm silicon wafer by a photolithography and deep reactive ion etching [Figs. 2(b) and 2(c)]. To make the surface hydrophobic, all of the samples were spin-coated with Teflon AF solution (DuPont). The post and grate patterns were selected for their geometric simplicity and a convenient comparison with both the wetting-transition theory [20,21] and the

numerical [11–19] or experimental [9,10] slip data available. The grates were designed to be concentric so that they were parallel to the liquid flow in the rheometer system. It is critical to report that a sample surface needed to be free of any defect over the entire test area to allow slip tests over the range pursued in this study. For example, a liquid was most likely to proceed to the crevices formed by defects, initiating a wetting transition. Once a wetting occurred, we observed a significant increase in the torque so that such test runs were aborted. The state of nonwetting was visually confirmed after each run to validate the data. A dedicated microfabrication procedure has been developed to produce such near-perfect samples, as described in the supplementary material [23].

The dominant errors in the rheometry measurement are the edge or end effects [7,22], resulting from either a deviation in the amount of filling liquid or a varying contact angle according to the surface condition. To minimize the errors from the edge or end effects, the position and curvature of the liquid meniscus were carefully controlled in this study by implementing a ring of trench on every sample along the outer boundary of a test section. This trench anchors the contact line of the meniscus at its sharp top edge, so that the position of the meniscus is not affected by the surface conditions. The curvature of the meniscus is then controlled by manually adjusting the liquid volume after the cone is in place. The shape of the free surface (meniscus) was then monitored by a high-speed camera during measurement (Fig. 3). From the images, the deviation in the shearing radius was estimated to be much less than 0.1 mm (or 7 μm in slip length), validating the accuracy of the rheometer system for the measurement of relatively large slips.

First, to investigate the effect of the gas fraction on the slip, slip lengths were measured on samples with fixed pitch of 50 μm but varying gas fractions—target gas fractions of 50%, 85%, 95%, 98%, 99%, and 99.5% for posts and 50%, 85%, 95%, and 98% for grates [24]. For all of the samples, the depth was maintained as the same as the
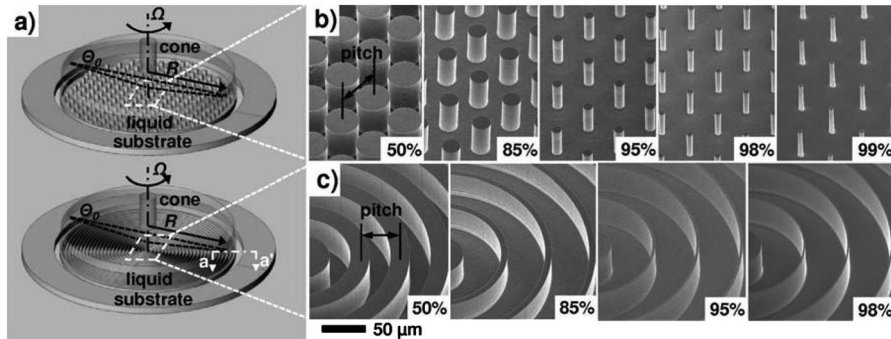
FIG. 2.   (a) Schematic description of a rheometer test. A rotating cone imposes a constant shear rate over a test section with either posts or grates. Torque applied to the cone by the sheared liquid on a substrate is recorded and used to estimate the slip length. (b) Scanning electron microscopy (SEM) images of post patterns with 50 μm pitch and the following target gas fractions: 50%, 85%, 95%, 98%, and 99%. (c) SEM images of grate patterns with 50 μm pitch and the following target gas fractions: 50%, 85%, 95%, and 98%. The direction of grates coincides with the direction of liquid flow generated by the cone rotation.
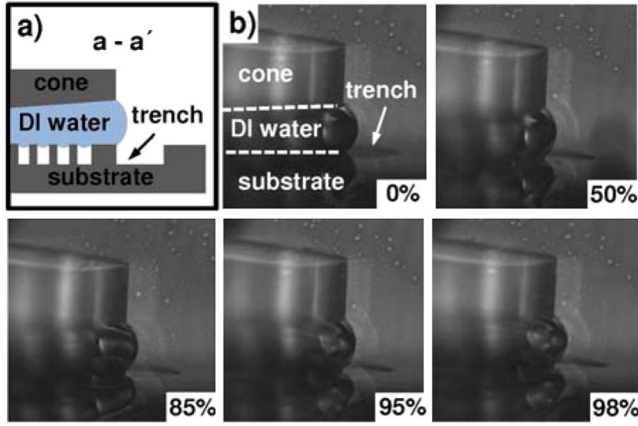
FIG. 3 (color online). (a) Cross section of a ring of trench along the outer boundary of the test section implemented to control the position of the meniscus contact line (Not drawn to scale). See Fig. 2(a) for the location of cross section a-a′. (b) Images of the free surfaces (menisci) of shearing water at the edge of cone-and-plate system having grating patterns of 50 μm pitch and the following target gas fraction: 0 (flat surface), 50%, 85%, 95%, and 98%.

pitch (i.e., 50 μm). All of the slip lengths were collected, and the averages are shown in Fig. 4(a) along with the theoretical predictions available for posts [19] and grates [12]. Overall, the slip length exponentially increased as the gas fraction approached unity (100%), agreeing well with the theory [12,19]. On posts, the slip length increased more rapidly in the high gas fraction range than on grates, in accord with the analytical scaling law [19] represented by

$$\delta \sim L/\sqrt{1 - \phi_g}\,(\text{posts}), \quad \delta \sim L\log(1 - \phi_g)(\text{grates}). \quad (4)$$

The discrepancy of the experimental data from the theoretical value for posts is considered to be due to the rotational flow pattern in the rheometer system, where the flow direction varies continuously relative to the underlying grid pattern of posts. In comparison, the rotational flow stays parallel to the concentric grate patterns, and the discrepancy between the experimental and theoretical values was not significant (less than 3 μm). Since the flow driven by the rotating cone maintains a uniform shear rate over the sample surface, the flow on the concentric grooves in the rheometer test closely resembles the simple flow parallel to the linear grooves, on which the theory is based. In fact, our experimental results agreed well with the previous experimental study [9] and corresponding theoretical values, both for linear grooves. For example, the ratio of slip length to pitch was 0.2–0.3 at the gas fraction between 50% and 80% in Ref. [9], while our experimental results showed that this ratio was 0.15 at 50% gas fraction and over 0.3 at the gas fraction over 85%. The close agreement with the previous experimental study and the theoretical values validates the fact that there would be no significant influence on the slip by the axisymmetrical configuration in the rheometer system.
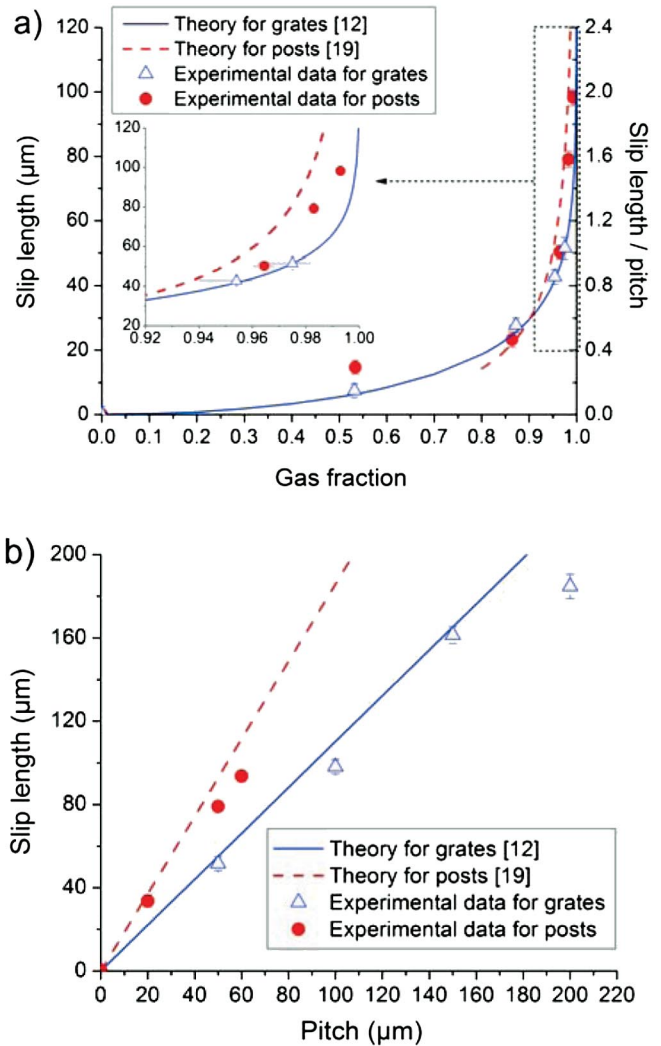
FIG. 4 (color). (a) The effect of gas fraction on the slip length with the pitch fixed at 50 μm. The horizontal error bar through the averaged data represents the uncertainty of gas fraction due to the structures' geometric variation over the entire sample area, while the vertical error bar represents the standard deviation in the measured data. (b) The effect of pitch on the slip length with the gas fraction fixed at 98%.

As opposed to Ref. [8], the data for posts show that the maximum slip is not always limited by the lateral scale of the surface structures. Instead, the maximum slip is constrained by the stability condition for a dewetted state. For our test (i.e., the pressure range of 200–300 Pa), the stability condition for posts predicts that the wetting transition occurs at the gas fraction of 99.4% when the pitch is 50 μm. Agreeing well with this prediction, we could maximize the slip effect by increasing the actual gas fraction up to 99.3% (§ in Fig. 1) (or a target gas fraction of 99%), when the slip length of ~100 μm (twice as large as the pitch of 50 μm) was achieved [Fig. 3(a)]. At the gas fraction of 99.7% (or target fraction of 99.5%), we observed the wetting transition as predicted by the theory, and the surface lost its superhydrophobicity as recorded as

"wetting (post)" in Fig. 1. Our results imply that a slip length several times as large as the pitch would be possible for posts if the pitch was submicron as demonstrated in our previous report [7].

Second, to investigate the effect of pitch on slip, slip lengths were measured on samples with the target gas fraction fixed at 98% but with varying pitches—20, 50, and 60 μm for posts and 50, 100, 150, 200, and 250 μm for grates. The depth for each sample was maintained to be the same as the corresponding pitch. The averaged slip lengths are shown in Fig. 4(b) along with theoretical predictions [12,19]. On both post and grate patterns, the slip increased linearly with the pitch. This result illustrates that, in addition to the high gas fraction, the larger pitch can produce a more pronounced slip effect, although the functional dependence is weaker. Similar to the gas fraction, the maximum pitch for posts and grates is limited by the condition for the wetting transition. For example, at the gas fraction of 98% and pressure of ~300 Pa, the maximum pitch for posts avoiding the transition to wetting would be ~60 μm according to the theory (# in Fig. 1). On the other hand, at the same gas fraction and pressure, grates would allow larger pitches, up to 230 μm (* in Fig. 1). At 200 μm pitch († in Fig. 1), very close to the theoretical limit, we succeeded in obtaining the largest slip of 185 μm [Fig. 4(b)], a giant slip 10 times larger than the previous maximum [7,9]. We noted that the slip length of 185 μm was a little lower than the theoretical prediction (~210 μm). It is speculated that the pitch became so large and comparable to a cone-and-plate gap size that a perturbation from the patterned sample may extend to the opposite cone wall, limiting slip length in such a Couette flow configuration [14]. At the pitch of 250 μm, wetting occurred over the entire area of the sample as recorded as "wetting (grate)" in Fig. 1, agreeing well with the theoretical thermodynamic prediction for our experimental condition (i.e., pressure of 200–300 Pa).

In summary, through the independent control of surface parameters, we have verified that the slip on a structured surface increases exponentially with gas fraction and linearly with pitch. Enabled by the precisely defined and defect-free microstructured surfaces, our experimental results approached the theoretical thermodynamic limits for a dewetting surface condition and demonstrated unprecedentedly large slips, up to 185 μm. The results confirmed that a high gas fraction and a large pitch within the thermodynamic boundary of the Cassie state are two key surface parameters of superhydrophobic surfaces for a maximized slip effect. The giant slip observed in this Letter is larger than the length scale of many microfluidic systems and approaches that of regular (macroscopic) systems for the first time. For example, the boundary-layer thickness in many high-Reynolds-number liquid flows (e.g., around underwater vehicles) is on the order of a millimeter, for which a slip length close to 200 μm will make a significant impact in drag reduction [7].

[1] C.-H. Choi, K. J. A. Westin, and K. S. Breuer, Phys. Fluids **15**, 2897 (2003); C. Neto, D. R. Evans, E. Bonaccurso, H. Butt, and V. S. J. Craig, Rep. Prog. Phys. **68**, 2859 (2005); E. Lauga, M. P. Brenner, and H. A. Stone, in *Handbook of Experimental Fluid Dynamics*, edited by J. Foss, C. Tropea, and A. Yarin (Springer, New York, 2007).

[2] M. Majumder, N. Chopra, R. Andrews, and B. J. Hinds, Nature (London) **438**, 44 (2005); J. K. Holt *et al.*, Science **312**, 1034 (2006).

[3] J. Kim and C.-J. Kim, in *Proceedings of the 15th IEEE International Conference on Micro Electro Mechanical System* (IEEE, Piscataway, NJ, 2002), p. 479.

[4] K. Watanabe and H. Udagawa, J. Fluid Mech. **381**, 225 (1999).

[5] A. K. Balasubramanian, A. C. Miller, and O. K. Rediniotis, AIAA J. **42**, 411 (2004).

[6] S. Gogte *et al.*, Phys. Fluids **17**, 051701 (2005).

[7] C.-H. Choi and C.-J. Kim, Phys. Rev. Lett. **96**, 066001 (2006).

[8] P. Joseph *et al.*, Phys. Rev. Lett. **97**, 156104 (2006).

[9] J. Ou, B. Perot, and J. P. Rothstein, Phys. Fluids **16**, 4635 (2004); J. Ou and J. P. Rothstein, *ibid.* **17**, 103606 (2005).

[10] C.-H. Choi, U. Ulmanella, J. Kim, C. Ho, and C.-J. Kim, Phys. Fluids **18**, 087105 (2006).

[11] C. Cottin-Bizonne, J.-L. Barrat, L. Bocquet, and E. Charlaix, Nature Mater. **2**, 237 (2003).

[12] E. Lauga and H. A. Stone, J. Fluid Mech. **489**, 55 (2003).

[13] C. Cottin-Bizonne *et al.*, Eur. Phys. J. E **15**, 427 (2004).

[14] N. V. Priezjev, A. A. Darhuber, and S. M. Troian, Phys. Rev. E **71**, 041608 (2005).

[15] R. Benzi *et al.*, J. Fluid Mech. **548**, 257 (2006).

[16] J. Davies, D. Maynes, B. W. Webb, and B. Woolford, Phys. Fluids **18**, 087110 (2006); D. Maynes, K. Jeffs, B. Woolford, and B. W. Webb, *ibid.* **19**, 093603 (2007).

[17] M. Sbragaglia and A. Prosperetti, Phys. Fluids **19**, 043603 (2007).

[18] M. Sbragaglia *et al.*, Phys. Rev. Lett. **97**, 204503 (2006); C. Kunert and J. Harting, *ibid.* **99**, 176001 (2007).

[19] C. Ybert *et al.*, Phys. Fluids **19**, 123601 (2007).

[20] N. A. Patankar, Langmuir **20**, 7097 (2004); L. Barbieri, E. Wagner, and P. Hoffmann, *ibid.* **23**, 1723 (2007).

[21] C. W. Extrand, Langmuir **20**, 5013 (2004); **22**, 1711 (2006); Q. S. Zheng, Y. Yu, and Z. H. Zhao, *ibid.* **21**, 12 207 (2005).

[22] C.-H. Choi and C.-J. Kim, Phys. Rev. Lett. **97**, 109602 (2006).

[23] See EPAPS Document No. E-PRLTAO-101-069832 for the derivation of Eq. (3) and the detailed microfabrication procedure. For more information on EPAPS, see http://www.aip.org/pubservs/epaps.html.

[24] For grates, the variation in linewidth over the sample area—a photolithographic limit—prevented us from going below 1 μm in feature size, limiting the gas fraction to 98%, when the slip length of ~50 μm was achieved.